J Therm Anal Calorim (2011) 104:781–788
DOI 10.1007/s10973-010-1008-1

Physicochemical properties of non-stoichiometric oxides

Mixed conductors: Part II

A. Caneiro · L. Mogni · N. Grunbaum · F. Prado

Received: 18 May 2010 / Accepted: 5 August 2010 / Published online: 29 August 2010

Abstract One of the most important challenges with solid oxide fuel cells (SOFC) is to find cathode materials with high enough catalytic activity for the dissociation of the molecular oxygen. Oxide mixed conductors with the perovskite structure (ABO_3) and high Co content in the B site have been extensively studied to be used as cathode in SOFC. This is the second part of a review of high temperature properties of two mixed conductors systems. The first part was focused on the $n = 2$ $Sr_3FeMO_{6+\delta}$ (M = Fe, Co, Ni) Rudlesdden Popper phases, while in this paper we discuss the thermodynamic and transport properties of the perovskite solid solution $Sr_{1-x}La_xFe_{0.2}Co_{0.8}O_{3-\delta}$ ($0 \leq x \leq 0.4$) in the temperature range $773 \leq T \leq 1173$ K. In particular, the interest has been focused on the $x = 0$ sample, which exhibits large ionic conductivity values ($\sigma_i \sim 1$ S cm^{-1}), but suffers a structural transformation from cubic to orthorhombic symmetry because the ordering of the oxygen vacancies when the oxygen partial pressure decreases. Measurements of the oxygen chemical potential (μ_{O_2}) as function of oxygen content and temperature, coupled with high temperature X-ray diffraction data, permitted us to broaden the knowledge of the T–δ–$p(O_2)$ phase diagram for the $x = 0$ sample. In addition, we have investigated the effects of the La incorporation on the stability range of the cubic phases of the $Sr_{1-x}La_xFe_{0.2}Co_{0.8}O_{3-\delta}$ solid solution.

Keywords Perovskites · Brownmillerite · Mixed conductors · Phase diagrams

A. Caneiro (✉) · L. Mogni · N. Grunbaum · F. Prado
Centro Atómico Bariloche, CNEA, 8400 San Carlos de Bariloche, Argentina
e-mail: caneiro@cab.cnea.gov.ar

A. Caneiro
CNEA—Comisión Nacional de Energía Atómica-Argentina, Centro Atómico Bariloche, San Carlos de Bariloche, Argentina

A. Caneiro · L. Mogni
CONICET—Consejo Nacional de Investigaciones Científicas y Técnicas, Centro Atómico Bariloche, San Carlos de Bariloche, Argentina

F. Prado
CONICET—Consejo Nacional de Investigaciones Científicas y Técnicas, Universidad Nacional de Sur, Bahía Blanca, Argentina

Introduction

Oxide mixed conductors exhibiting both electronic and ionic conductivity have attracted much attention in the last years due to their potential application in high temperature electrochemical devices such as electrodes for solid oxide fuel cells (SOFC), oxygen separation membranes, and methane conversion reactors [1, 2].

Fuel cells (FC) are one of the most efficient systems to produce electrical energy from hydrogen and hydrocarbons [3]. These devices allow the direct conversion of chemical energy (Gibbs free energy) into electrical energy from the electrochemical oxidation of gases such as H_2, CO, CH_4, C_3H_8, C_4H_{10} etc. [4].

Between the different types of fuel cells, the SOFC are extensively studied since they do not only require the use of pure gases like H_2, CO can also be used as fuel and its efficiency can be improved using the heat ($T\Delta S$) produced in the oxidation reaction to generate steam (co-generation). The efficiency of the SOFC in the co-generation form can reach values as high as 70%. However, the high operation temperatures of the SOFC ($T > 1173$ K) require ceramic

materials for the electrolyte, cathode, anode, and interconnection materials. One of the disadvantages of the SOFC is the high cost of the interconnection material (lanthanum chromites) and the present challenge is to reduce the operation temperature in order to replace lanthanum chromites by less expensive materials such as stainless steel. FC operating at temperatures below 973 K are named intermediate temperature solid oxide fuel cells (IT-SOFC). However, this lower operating temperature requires new suitable materials for the electrolyte and electrodes.

Cathodes for IT-SOFC are widely investigated since the reduction of the molecular oxygen according to the whole reaction $1/2O_2 + 2e \rightarrow O^{2-}$ is the main process that limits the efficiency of the IT-SOFC. It is worth mentioning that under working conditions, the main potential loss is caused by the overpotential at the cathode.

The state of the art of the SOFC uses lanthanum manganites ($La_{1-x}Sr_xMnO_3$) as cathode materials. In this case, the electrode reaction takes place at the triple phase boundary (TPB), gas phase/electrolyte/electrode. The gas phase provides the O_2, the electrode the electrons and the electrolyte the oxygen vacancies for O^{2-} ions incorporation. Lanthanum manganites cannot be used for cathodes in IT-SOFC since the reduction of the operation temperature generates large overpotentials.

Mixed conductors (MIEC) are suitable materials for this purpose, because the simultaneous presence of electronic plus ionic conductivity enlarges the reaction zone beyond the TPB with the consequent reduction of the cathode overpotentials. Most of the mixed conductors pointed out as candidates to be used as cathode in IT-SOFC are transition metal oxides with perovskite or perovskite related crystal structures that exhibit oxygen non-stoichiometry.

The electronic conductivity of mixed conductors is mainly related to the mixed valence of the transition metals whereas the ionic conductivity is due to the presence of mobile oxygen vacancies at high temperatures. Mixed conductor oxides are among the group of materials in which the oxygen content plays a fundamental role on their specific properties. This review is complementary to a previous one devoted to present another family of non-stoichiometric oxides, the superconducting oxides [5].

In the case of oxide mixed conductors used as cathode material, it seems evident that the cathode reaction should be related to the defect structure of the transition metal oxides. Besides, the high temperature properties of these materials can be affected by structural transformations occurring under the working conditions. For this reason, the resolution of the phase diagram of SOFC materials results very important in the understanding of these properties.

The thermal analysis involves powerful methods that permit the evaluation of the defect structure [6–10] and structural transformations [11, 12] of non-stoichiometric oxides used in combination with data obtained from high temperature XRD. Also it is possible to study, trough thermal analysis, the thermodynamic properties and the chemical stability of diverse systems [13, 14].

This Part II of this review devoted to oxide mixed conductors is focused on the perovskite solid solution $Sr_{1-x}La_xFe_{0.2}Co_{0.8}O_{3-\delta}$ with $0 \leq x \leq 0.4$. Thermogravimetric (TG) measurements along with the high temperature X-ray diffraction (HT-XRD) permitted us to obtain a more detailed phase diagram of $SrFe_{0.2}Co_{0.8}O_{3-\delta}$ compound. This compound undergoes a phase transition from a disordered cubic to an ordered orthorhombic phase with the consequence loss of oxygen conductor properties. However, the subsequence studies of $Sr_{1-x}La_xFe_{0.2}Co_{0.8}O_{3-\delta}$ system with $0 \leq x \leq 0.4$ shown that the substitution of Sr^{2+} by La^{3+} prevents this phase transition.

Experimental

Samples of the perovskite solid solution $Sr_{1-x}La_xFe_{0.2}Co_{0.8}O_{3-\delta}$ with $0 \leq x \leq 0.4$ were prepared following the solid state reaction method with stoichiometric quantities of highly pure $SrCO_3$, Fe_2O_3, Co_3O_4. The raw materials were weighed and then ground in a ball mill for 1 h. The powder was calcined at 1223 K in air for 12 h. The final treatment for this compound was 1423 K for a period of 12 h with an intermediate grinding.

The presence of single phase materials, with cubic symmetry (S.G. *Pm3m*) for $Sr_{1-x}La_xFe_{0.2}Co_{0.8}O_{3-\delta}$ was checked by powder XRD. No evidence of secondary phases was detected. The homogeneity of the samples was confirmed by SEM observations and EDS analysis.

Thermogravimetric measurements (TG) under controlled $p(O_2)$ were performed using a highly sensitive thermogravimetric equipment [15, 16] consisting of a symmetrical thermobalance based on a Cahn 1000 electrobalance coupled to an electrochemical gas blending system. The electrochemical system is composed of an electrochemical oxygen pump and an oxygen sensor. The electrochemical pump provides Ar–O_2 mixtures and the oxygen sensor determines the $p(O_2)$. Mixtures of Ar–O_2 with $p(O_2)$ within the range $10^{-5} < p(O_2) < 1$ atm. can be easily prepared by only changing the electrical current applied to the oxygen pump.

The thermobalance allows the determination of sample mass changes within ± 10 μg, i.e., for oxide samples of about 0.6 g ($Sr_{1-x}La_xFe_{0.2}Co_{0.8}O_{3-\delta}$) changes on the oxygen content within ± 0.0003 can be detected.

The equilibrium criterion used for our measurements, verified over a period of 24 h, was constant mass samples

within 10 mg. A more detailed description of this thermobalance can be found in Ref. [5]

After performing the TG measurements under controlled $p(O_2)$, the absolute oxygen content of the samples was determined in situ by reduction in dry H_2 at 1273 K. SrO, La_2O_3, and metallic Co and Fe were the final products depending on the composition of the compound.

DC resistivity measurements at high temperature and controlled $p(O_2)$ were carried out by a standard four-probe method on rectangular samples with dimensions 1.5 mm × 5 mm × 20 mm.

For high temperature X-ray diffraction (HT-XRD) the sample was spread on a resistively heated platinum ribbon mounted in an Anton Paar HTK-10 camera coupled to the diffractometer. The $p(O_2)$ within the camera was controlled by means of flowing N_2–O_2 mixtures supplied by the electrochemical system.

Results and discussion

The $SrCoO_{3-\delta}$ compound crystallizes in the R32 hexagonal symmetry. The substitution of Co by Fe changes the hexagonal symmetry to cubic, which increases the oxygen permeability to values as high as 10^{-6} mol cm^{-2} s^{-1} at 1173 K for $SrCo_{0.8}Fe_{0.2}O_{3-\delta}$ [17]. The cubic or pseudo-cubic structure (C) of the $SrCo_{0.8}Fe_{0.2}O_{3-\delta}$ material [18] is stable at the temperature range $550 < T < 1173$ K for $p(O_2) > 0.209$ atm., where it exhibits a wide range of oxygen non-stoichiometry with $3-\delta$ ranging between 2.43 and 2.65 [19]. In Fig. 1a, the crystal structures of a cubic the ABO_3 is shown. On the other hand, the brownmillerite phase (O) with orthorhombic symmetry (space group Icmm) displays a narrow range of oxygen non-stoichiometry around 2.5. The crystal structure of the brownmillerite phase is related to that of the perovskite phase. While the ABO_3 perovskite phase consists of a three-dimensional network of BO_6 octahedra, the $ABO_{2.5}$ brownmillerite phase has a layer of BO_6 octahedra alternating with a layer of BO_4 tetrahedra along the *b*-axis, as shown in Fig. 1b, resulting in tetragonal or orthorhombic symmetry. However, the brownmillerite phase transforms to cubic phases at high temperatures due to a thermal disordering of the oxygen vacancies [20, 21]. This phase transformation involves a significant volume change which is of critical importance in methane conversion reactors as they can lead to mechanical fracture.

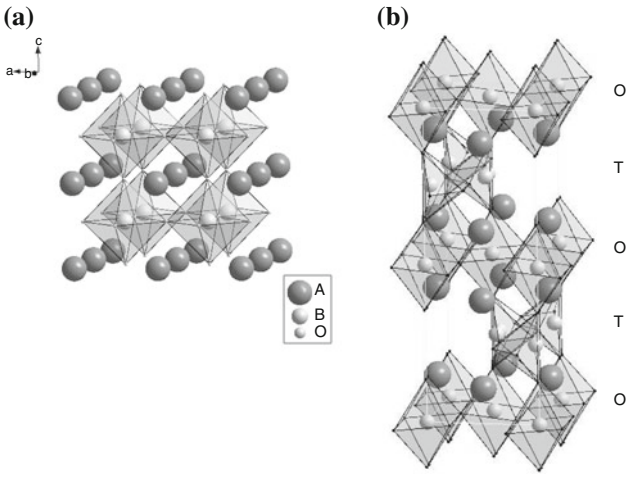

Fig. 1 **a** Crystal structure of ABO_3 (S.G. *Pm*-3*m*). **b** Crystal structure of the brownmillerite phase $A_2B_2O_5$ with Icmm crystal symmetry

$SrFe_{0.2}Co_{0.8}O_{3-\delta}$ perovskite

In Fig. 2, the TG measurements of the equilibrium $p(O_2)$ are plotted as a function of the oxygen content at 823 and 1023 K for the $SrFe_{0.2}Co_{0.8}O_{3-\delta}$ compound ($x = 0$). The isotherms were performed under reduction (decreasing $p(O_2)$) and subsequent oxidation (increasing $p(O_2)$).

Both isotherms are qualitatively similar, despite the presence of hysteresis in the 1023 K isotherm.

For the 1023 K isotherm, the starting point A was obtained by annealing the sample in pure O_2 at 1 atm. during 24 h. The different parts of this isotherm are briefly described as follows:

- Part A–B: Data points between A and B were obtained under subsequent reduction of the sample. The oxygen content of point B is $3 - \delta = 2.517$ at $p(O_2) = 4.1 \times 10^{-3}$ atm.
- Part B–C: Decreasing $p(O_2)$ slightly below point B, the weight loss kinetic was appreciably slower than that of the A–B part. The time to reach equilibrium for point C was approximately 2 days.

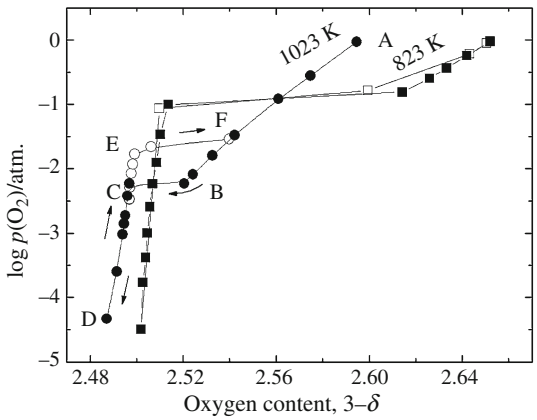

Fig. 2 log $p(O_2)$/atm. versus $3 - \delta$ plots at 823 and 1023 K for $SrCo_{0.8}Fe_{0.2}O_{3-\delta}$. *Closed* and *open symbols* correspond to the reduction and oxidation processes, respectively [22]

- Parts C–D and D–E: The equilibrium data points between points C and D (*close symbols*) were obtained decreasing successively $p(O_2)$ and the data points represented by open symbols between points D and E increasing successively $p(O_2)$.
- Part E–F: After a slight increment in $p(O_2)$ beyond point E, the sample began to oxidize slowly reaching point F after 2 days.
- Part F–A: Points in part F–A were obtained increasing $p(O_2)$. The value reached at 1 atm. agrees with the starting point A. This fact indicates that no evaporation of the sample at 1023 K took place despite the long period required for the equilibrium $p(O_2)$ measurements. On the other hand, the overlap between points of part A-B and F–A indicates that these points represent thermodynamic equilibrium states.

The 1023 K isotherm exhibits three well-differentiated regions. Part A–B reveals the presence of a non-stoichiometric phase with a wide range of oxygen contents. On the contrary, part D–E indicates the presence of an almost stoichiometric compound. Nearly constant $p(O_2)$ values for parts B–C and E–F indicate the existence of a two-phase field in agreement with the Gibbs's rule. However, we noted the presence of substantial hysteresis in the $p(O_2)$ values within the two-phase field region.

In Fig. 2, the $p(O_2)$ isotherm obtained at 823 K is also included. The shape of this isotherm is qualitatively similar to that determined at 823 K. However, the hysteresis for this isotherm is negligible.

The shape of these isotherms undoubtedly indicates the nature of the phase diagram of the $SrCo_{0.8}Fe_{0.2}O_{3-\delta}$ compound. The A–B part denotes the presence of the non-stoichiometric cubic phase (C) while part D–E corresponds to the stabilization of the brownmillerite $Sr_2Co_{1.6}Fe_{0.4}O_5$ phase with orthorhombic symmetry (O).

The isotherm parts B–C and E–F correspond to the precipitation of the brownmillerite phase from the cubic phase and the precipitation of the cubic phase from the brownmillerite, respectively.

The cubic phase accepts a wide range of oxygen non-stoichiometry by creation of oxygen vacancies randomly distributed in the structure. These defects are responsible for the presence of ionic conductivity, which in addition to the electronic conductivity, make this material a mixed conductor and therefore suitable for applications as cathode materials in IT-SOFC [17–19].

The brownmillerite phase precipitates from the cubic phase because of the ordering of oxygen vacancies along the $[101]_p$ direction in alternating (010) perovskite planes producing a $\sqrt{2}\,a_p \times 4a_p \times \sqrt{2}\,a_p$ supercell. The oxygen ordering leads to a layer structure in which BO_6 octahedra alternate with BO_4 tetrahedra along the *c*-axis [23].

The presence of hysteresis in non-stoichiometric oxides has been extensively discussed in the literature. This behavior is related to the existence of two phases with close compositions and related structures, which is the case for the cubic and the orthorhombic phase of the $SrFe_{0.2}Co_{0.8}O_{3-\delta}$ material. Under theses conditions, it may be possible to create coherent or semi-coherent interfaces due to the presence of crystallographic planes of low lattice mismatch. These interfaces are characteristic by low interfacial energies despite their non-negligible strain energy (ΔG_S). The thermodynamic description of the two-phase system (the cubic and the orthorhombic) requires the incorporation of the ΔG_S contribution. This contribution to the total free energy of the system makes the Gibbs's rule system invalid, giving multivaluated $p(O_2)$ values for the two-phase region [24–26].

The data shown in Fig. 2 indicate that the hysteresis increases along with *T*. Therefore, this phenomenon is not associated to any thermal activated process; otherwise the trend of the hysteresis loop should be the opposite. We believe that the dependence of hysteresis on *T* is due to the fact that the compositional differences between both phases (oxygen content) decrease with *T* and thereby increase the possibility to form coherent or semi-coherent interfaces.

Despite the presence of hysteresis, it is possible to determine with high accuracy the phase boundaries between the C phase and the two phase field region (C/C + O) and the small oxygen stoichiometric range of the O brownmillerite phase from the $p(O_2)$ isotherms.

In Fig. 3, all the $p(O_2)$ isotherms for *T* between 823 and 1223 K are plotted. For clarity, only the values obtained under reduction conditions are included.

The $p(O_2)$ data clearly show that the $p(O_2)$ plateau, indicative of the existence of a two phase-field region, is absent for $T > 1023$ K in agreement with literature [19].

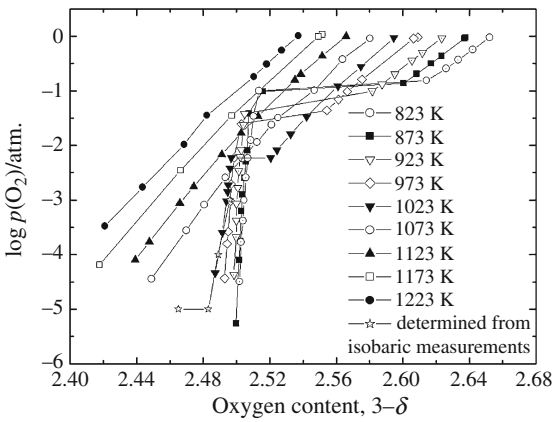

Fig. 3 log $p(O_2)$/atm. versus $3 - \delta$ plots for $SrCo_{0.8}Fe_{0.2}O_{3-\delta}$ at several temperatures (data corresponding to the reduction process) [22]

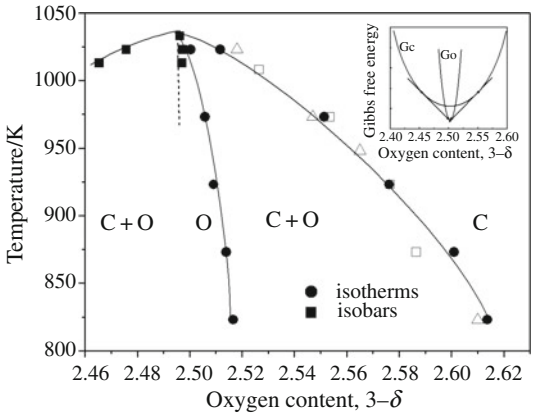

Fig. 4 Phase diagram of $SrCo_{0.8}Fe_{0.2}O_{3-\delta}$. Experimental data from (*closed circle*) isothermal measurements, (*closed square*) isobaric measurements, (*open triangle*) Ref. [19], and (*open square*) Ref. [27]. The *inset* shows the schematic free energy-composition curves for the cubic and orthorhombic phases at a given T lower than 1023 K [22]

Therefore, at $T > 1023$ K the cubic phase is stable in the whole range of $p(O_2)$. From these $p(O_2)$ measurements complemented with TG isobars (measurements under constant $p(O_2)$), the phase diagram for the $SrFe_{0.2}Co_{0.8}O_{3-\delta}$ compound was built. A more detailed description of this study can be found in Ref. [22].

In Fig. 4, the phase diagram (T versus oxygen content) for $SrFe_{0.2}Co_{0.8}O_{3-\delta}$ obtained from our TG measurements is shown. Literature data are also included in this figure.

The (C + O)/C and the O/(C + O) (●) phase boundaries, at the rich oxygen content side, were obtained from isothermal measurements, while the (C + O)/C and the C/(C + O) phase boundaries, at the poor oxygen content side (■) were determined from isobaric measurements. In the inset of this figure, a schematic diagram of the free energy curves versus composition for the C and O phases is drawn. The free energy curve of the cubic phase shows a broad dependence on composition while that of the orthorhombic phase displays a narrow range of oxygen non-stoichiometry. The common tangent between both free energy curves defines the phase boundaries in the temperature versus composition phase diagram.

From the equilibrium $p(O_2)$ data, the oxygen chemical potential, μ_{O_2}, can be computed using the following equation:

$$\mu_{O_2} = \mu_{O_2}^{\text{oxide}} = \mu_{O_2}^{\text{ref}} + RT \ln p(O_2)/p(O_2)^{\text{ref}}) \quad (1)$$

where R is the gas constant, $p(O_2)^{\text{ref}} = 1$ atm and $\mu_{O_2}^{\text{ref}}$ is the oxygen chemical potential of the reference gas obtained from thermodynamic tables [28].

From the μ_{O_2} data, the partial molar enthalpy h_{O_2} and the partial molar entropy s_{O_2} can be determined by means of the following relations:

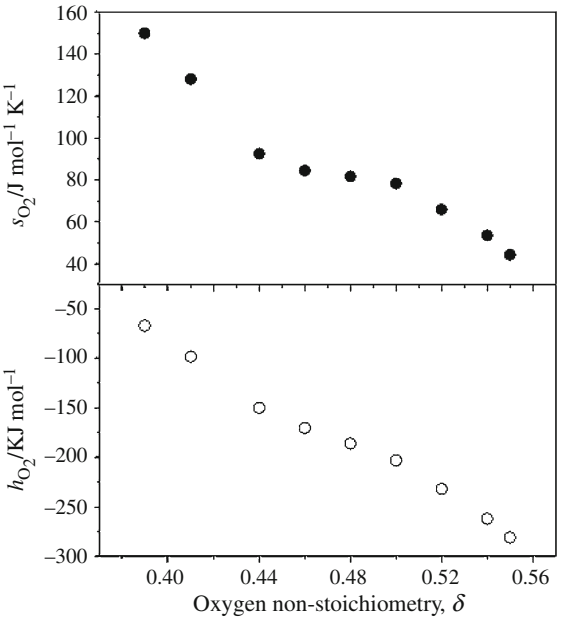

Fig. 5 Plots of s_{O_2} and h_{O_2} as a function of the oxygen content for $SrCo_{0.8}Fe_{0.2}O_{3-\delta}$ [22]

$$s_{O_2} = -\left.\frac{\partial \mu_{O_2}}{\partial T}\right|_{\delta} \quad (2)$$

$$h_{O_2} = \left.\frac{\partial (\mu_{O_2}/T)}{\partial (1/T)}\right|_{\delta} \quad (3)$$

The values of s_{O_2} and h_{O_2} for the cubic phase are displayed in Fig. 5.

Useful information can be extracted from the dependence of both thermodynamic quantities on the oxygen content. It can be observed that h_{O_2} and s_{O_2} decrease with increasing oxygen content. The variation of s_{O_2} with δ is in opposition with that observed for $La_{1-x}Sr_xCoO_{3-\delta}$ [29, 30] where s_{O_2} increases with δ. We attribute this difference in the behavior of s_{O_2} to the different oxygen non-stoichiometry range analyzed for both compounds. The $La_{1-x}Sr_xCoO_{3-\delta}$ compound exhibits a smaller oxygen vacancies concentration than $SrFe_{0.2}Co_{0.8}O_{3-\delta}$. Therefore, the behavior of s_{O_2} for $La_{1-x}Sr_xCoO_{3-\delta}$ can be explained using the ideal solution model [29]. On the contrary, the high concentration of oxygen vacancies of $SrFe_{0.2}Co_{0.8}O_{3-\delta}$, might lead to the formation of ordered regions such as clusters or microdomains in the oxygen content range close to $3 - \delta = 2.5$ even well above the order transition temperature ($\sim$1023 K) lessening the configurational entropy respect to that of the ideal solution causing the observed dependence of s_{O_2} with δ. The high h_{O_2} values suggest a strong interaction among defects for the $SrFe_{0.2}Co_{0.8}O_{3-\delta}$ compound.

$Sr_{1-x}La_xFe_{0.2}Co_{0.8}O_{3-\delta}$ perovskite

Despite the fact that $SrFe_{0.2}Co_{0.8}O_{3-\delta}$ compound exhibits the highest ionic conductivity of the (Sr,La)(Co,Fe)$O_{3-\delta}$ system, this material tends to lose oxygen and decomposes at high temperature (1173 K) under reduced environments (N_2, CH_4). Furthermore, as we discussed in the previous section, the high concentration of oxygen vacancies of $SrFe_{0.2}Co_{0.8}O_{3-\delta}$ increases the electrostatic interaction among oxygen defects and, thereby, the precipitation of the oxygen ordered brownmillerite phase at $T \leq 1023$ K [20]. This phase transformation involves an appreciable volume change that affects both the mechanical stability and the ionic conductivity of $SrFe_{0.2}Co_{0.8}O_{3-\delta}$ [31], which represent serious drawbacks for using $SrFe_{0.2}Co_{0.8}O_{3-\delta}$ as electrode material or membrane for oxygen separation

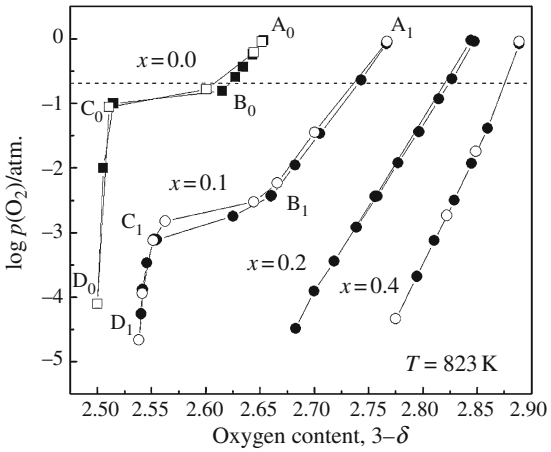

Fig. 6 Variations of the oxygen content with the equilibrium $p(O_2)$ at 823 K for the $Sr_{1-x}La_xCo_{0.8}Fe_{0.2}O_{3-\delta}$ ($0.0 \leq x \leq 0.4$) samples [32]. *Closed* and *open symbols* correspond to the reduction and oxidation processes, respectively

[20, 21]. On the other hand, the linear expansion coefficient of $SrFe_{0.2}Co_{0.8}O_{3-\delta}$ is much higher than that of the electrolytes $Ce_{0.9}Gd_{0.1}O_{1.95}$ (GGO) and $La_{0.8}Sr_{0.2}Ga_{0.83}Mg_{0.17}O_{2.81}$ (LSGM) [31].

Although the partial substitution of Sr by La decreases the oxygen permeation flux across a membrane of $SrFe_{0.2}Co_{0.8}O_{3-\delta}$, it also depresses the $p(O_2)$ values for the crystal structure transformation as well as the linear expansion coefficient. Thus, the equilibrium $p(O_2)$ measurements result in an effective experimental technique to analyze the effect of La doping on the O/T transition.

In Fig. 6, the equilibrium $p(O_2)$ data obtained at $T = 823$ K for $Sr_{1-x}La_xFe_{0.2}Co_{0.8}O_{3-\delta}$ with $x = 0$, 0.10, 0.20, and 0.40 are plotted. Similar to the data presented for the $SrFe_{0.2}Co_{0.8}O_{3-\delta}$ perovskite, the presence of a plateau for the $x = 0$ and 0.10 samples indicates the coexistence of both the cubic and orthorhombic phases. In this figure segments, A_0–B_0 and A_1–B_1 correspond to the cubic phase, B_0–C_0 and B_1–C_1 to the coexistence of both phases, and C_0–D_0 and C_1–D_1 represent the equilibrium $p(O_2)$ data of the brownmillerite phase for the $x = 0$ and $x = 0.10$ samples, respectively.

The plateau is present around log $p(O_2) \sim -0.8$ and log $p(O_2) \sim -2.8$ for the $x = 0$ and 0.1 samples, respectively. The increment of La content decreases the oxygen non-stoichiometric range of the cubic phase and depresses the equilibrium $p(O_2)$ of the plateau. The plateau is absent for the $x = 0.2$ and 0.4 samples indicating that within this range of $p(O_2)$ the cubic phase is the only stable phase. These results are confirmed by HT-XRD measurement. In Fig. 7 are shown some representative diffractogram obtained by $x = 0.1$ and $x = 0.4$ samples under N_2 atmosphere. While the $Sr_{0.9}La_{0.1}Co_{0.8}Fe_{0.2}O_{3-\delta}$ compound exhibits the brownmillerite formation between 673 and

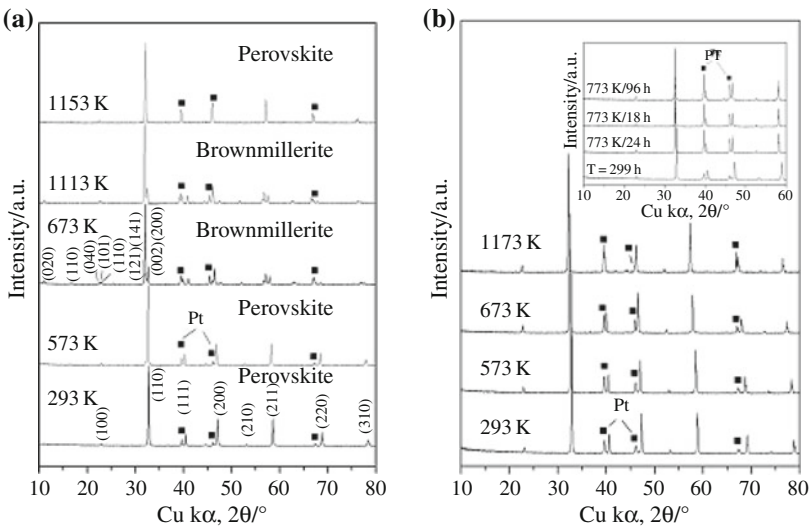

Fig. 7 X-ray diffraction patterns of **a** $Sr_{0.9}La_{0.1}Co_{0.8}Fe_{0.2}O_{3-\delta}$ and **b** $Sr_{0.6}La_{0.4}Co_{0.8}Fe_{0.2}O_{3-\delta}$ recorded at various temperatures in N_2 atmosphere

1113 K, the $Sr_{0.6}La_{0.4}Co_{0.8}Fe_{0.2}O_{3-\delta}$ presents a stable cubic structure for the overall temperature range.

The effect of the La content on the stabilization of the cubic phase can be understood by considering the charge balance in the $SrFe_{0.2}Co_{0.8}O_{3-\delta}$ perovskite. In the brownmillerite phase of composition $Sr_2Co_{1.6}Fe_{0.4}O_5$, the formal valence of the Co and Fe cations is +3. This valence gives an oxygen content of 5 and therefore a vacancy concentration of 1/6. Under these conditions, the free energy of the system is minimized by ordering the oxygen vacancies. The replacement of Sr by La modifies both the formal valence of the transition metals and the oxygen content values characteristic of the brownmillerite phase. The oxygen content of the brownmillerite phase with $x = 0.10$ is $\sim$2.55 and, then the formal valence of Co is $\sim$2.62 (assuming all the Fe as +3), which is below the +3 oxidation state of the Co ions in the $x = 0$ brownmillerite phase. Therefore, the oxidation state of Co and the oxygen vacancy concentration are modified as x increases and consequently the cubic phase is stabilized. A detailed discussion about these results can be found in Ref. [32].

Conclusions

- Isotherms and isobars of equilibrium $p(O_2)$ were determined by TG measurements for the $SrCo_{0.8}Fe_{0.2}O_{3-\delta}$ perovskite. The partial molar properties, s_{O_2} and h_{O_2}, for the cubic phase were computed from experimental data of the oxygen chemical potential μ_{O_2}. The dependence of both s_{O_2} and h_{O_2} with the oxygen content "$3 - \delta$" is discussed in terms of defect interactions and the provable presence of ordered domains at $T > 1023$ K. The T–$(3 - \delta)$ phase diagram of the $SrCo_{0.8}Fe_{0.2}O_{3-\delta}$ compound was reviewed and detailed determined within the oxygen content $(3 - \delta)$ ranging from 2.46 to 2.6. While the brownmillerite phase stabilizes at temperatures below 1073 K and exhibits a narrow stability around $3 - \delta = 2.5$, the cubic perovskite phase displays a broad range of oxygen non-stoichiometry between 2.46 and 2.6. For $T < 1073$ K, the cubic phase is separated from the orthorhombic phase by two phase regions at both sides of the orthorhombic phase.
- Equilibrium $p(O_2)$ measurements as a function of oxygen content "$3 - \delta$" at 823 K for the $Sr_{1-x}La_xCo_{0.8}Fe_{0.2}O_{3-\delta}$ are presented. The tendency to form the brownmillerite phase decreases with increasing La content, and the sample with $x = 0.4$ does not show any evidence of the formation of the brownmillerite phase under the conditions of this investigation.

Acknowledgements This work was supported by CNEA (Argentine Atomic Energy Commission), CONICET, and Universidad Nacional de Cuyo.

References

1. Skinner SJ. Recent advances in perovskite-type materials for solid oxide fuel cell cathodes. Int J Inorg Mater. 2001;3:113–21.
2. Bouwmeester HJ, Burggraf AJ. In: Gellings PJ, Bouwmeester HJ, editors. The CRC handbook of solid state electrochemistry. Boca Raton, FL: CRS Press; 1997.
3. Steel BCH, Heinzel A. Materials for fuel-cell technologies. Nature. 2001;414:345–52.
4. Larminie J, Dicks A. Fuel cells systems explained. 2nd ed. New York: Wiley; 2003.
5. Caneiro A, Prado F, Serquis A. Physical properties of non-stoichiometrics oxides: superconducting oxides. J Therm Anal Calorim. 2006;83(2):507–18.
6. González Arias A, Torres C, de Francisco C, Muñoz JM, Hernández Gómez P, Alejos O, Montero O, Iñiguez JI. Defect concentration in Ti-substituted YIG from TG curves. J Therm Anal Calorim. 2006;86(1):195–8.
7. Grzesik Z, Mrowec S. Kinetics and thermodynamics of point defects in non-stoichiometric metal oxides and sulphides. J Therm Anal Calorim. 2007;90(1):269–82.
8. Malta LFB, Caffarena VR, Medeiros ME, Ogasawara T. TA of non-stoichiometric ceria obtained via hydrothermal synthesis. J Therm Anal Calorim. 2004;75:901–10.
9. Aggarwal S, Töpfer J, Tsai T-L, Dieckmann R. Point defects and transport in binary and ternary, non-stoichiometric oxide. Solid State Ion. 1997;101–103:321–31.
10. Bishop SR, Duncan KL, Wachsman ED. Defect equilibria and chemical expansion in non-stoichiometric undoped and gadolinium-doped cerium oxide. Electrochim Acta. 2009;54(5):1436–43.
11. Hashimoto T, Yoshinaga M, Ueda Y, Komazaki K, Asaoka K, Wang S. Characterization of phase transition of $Ba_{2-x}Sr_xIn_2O_5$ by thermal analysis and high temperature X-ray diffraction. J Therm Anal Calorim. 2002;69:909–17.
12. Vashook VV, Zinkevich MV, Zonov YG, Kharton VV, Tsipis EV, Yaremchenko AA, Marozau IP, Viskup AP, Frade JR. Naumovich EN Phase relations in oxygen-deficient $SrCoO_{2.5-\delta}$. Solid State Ion. 1999;116(1–2):129–38.
13. Rycerz L, Ingier-Stocka E, Gadzuric S, Gaune-Escard M. Review of the thermodynamic and transport properties of EuBr2-RbBr binary system. J Therm Anal Calorim. 2010. doi:10.10007/s10973-010-0790-0.
14. Kumekawa Y, Hirai M, Kobayashi Y, Endoh S, Oikawa E, Hashimoto T. Evaluation of thermodynamic and kinetic stability of $CuAlO_2$ and $CuGaO_2$. J Therm Anal Calorim. 2010;99:57–63.
15. Caneiro A, Bonnat M, Fouletier J. Measurement and regulation of oxygen content in selected gases using solid electrolyte cells. IV. Accurate preparation of CO_2–CO and H_2O–H_2 mixtures. J Appl Electrochem. 1981;11:83–90.
16. Caneiro A, Bavdaz P, Fouletier J, Abriata JP. Adaptation of an electrochemical system for measurement and regulation of oxygen partial pressure to a symmetrical thermogravimetric analysis system developed using a Cahn 1000 electrobalance. Rev Sci Instrum. 1982;53:1072–5.
17. Qiu L, Lee TH, Liu L–M, Yang YL, Jacobson AJ. Oxygen permeation studies of $SrCo_{0.8}Fe_{0.2}O_{3-\delta}$. Solid State Ion. 1995;76:321–9.
18. Prado F, Armstrong T, Caneiro A, Manthiram A. Structural stability and oxygen permeation properties of $Sr_{3-x}La_xFe_{2-y}Co_yO_{7-\delta}$

($0 \leq x \leq 0.3$ and $0 \leq y \leq 1.0$). J Electrochem Soc. 2001;148: J7–14.
19. Liu LM, Lee TH, Qiu L, Yang YL, Jacobson AJ. A thermogravimetric study of the phase diagram of strontium cobalt iron oxide, $SrCo_{0.8}Fe_{0.2}O_{3-\delta}$. Mater Res Bull. 1996;31:29–35.
20. Kruidhof H, Bouwmeester HJM, van Doorn RHE, Burggraf AJ. Influence of order-disorder transitions on oxygen permeability through selected nonstoichiometric perovskite-type oxides. Solid State Ion. 1993;63–65:816–22.
21. Pei S, Kleefisch MS, Kobylinski TP, Faber J, Udovich CA, Zhang-McCoy V, Dabrowski B, Balachandran U, Mieville RL, Poeppel RB. Failure mechanisms of ceramic membrane reactors in partial oxidation of methane to synthesis gas. Catal Lett. 1994;30:201–12.
22. Grunbaum N, Mogni L, Prado F, Caneiro A. Phase equilibrium and electrical conductivity of $SrCo_{0.8}Fe_{0.2}O_{3-\delta}$. J Solid State Chem. 2004;177(7):2350–7.
23. Hodges JP, Short S, Jorgensen JD, Xiong X, Dabrowski B, Mini SM, Kimball CW. Evolution of oxygen-vacancy ordered crystal structures in the perovskite series Sr(n)Fe(n)O($3n - 1$) ($n = 2, 4, 8$, and ∞), and the relationship to electronic and magnetic properties. J Solid State Chem. 2000;151:190–209.
24. Knittel DR, Pack SP, Lin SH, Eyring L. A thermodynamic model of hysteresis in phase transitions and its application to rare earth oxide systems. J Chem Phys. 1977;67:134–42.
25. Inaba H, Pack SP, Lin SH, Eyring L. A kinetic study of oxidation of praseodymium oxides: PrO1.714+0.032 O2→PrO1.778. J Solid State Chem. 1980;33:295–304.
26. Porter DA, Easterling KE. Phase transformations in metals and alloys. London: Chapman & Hall; 1991.
27. Tikhonovich VN, Naumovich EN, Logvinovich DI, Kharton VV, Vecher AA. Oxygen deficiency and phase transitions in $SrCo_{1-x-y}Fe_xCr_yO_{3-\delta}$ ($x = 0.10$–0.40, $y = 0$–0.05). J Solid State Electrochem. 2003;7:77–82.
28. IUPAC. Commission on thermodynamics, "oxygen, international thermodynamic tables of the fluid state–9". Oxford: Blackwell Scientific; 1987.
29. Mizusaki J, Mima Y, Yamauchi S, Fueki K, Tawaga H. Nonstoichiometry of the perovskite-type oxides $La_{1-x}Sr_xCoO_{3-\delta}$. J Solid State Chem. 1989;80:102–11.
30. Mitberg EB, Patrakeev MV, Leonidov IA, Kozhevnikov VL, Poeppelmeier KR. High-temperature electrical conductivity and thermopower in nonstoichiometric $La_{1-x}Sr_xCoO_{3-\delta}$ ($x = 0.6$). Solid State Ion. 2000;130:325–30.
31. Huang K, Wan J, Goodenough JB. Oxide-ion conducting ceramics for solid oxide fuel cells. J Mater Sci. 2001;36:1093–8.
32. Prado F, Grunbaum N, Caneiro A, Manthiram A. Effect of La3+ doping on the perovskite-to-brownmillerite transformation in $Sr_{1-x}La_xCo_{0.8}Fe_{0.2}O_{3-\delta}$ ($0 \leq x \leq 0.4$). Solid State Ion. 2004; 167(1–2):147–54.